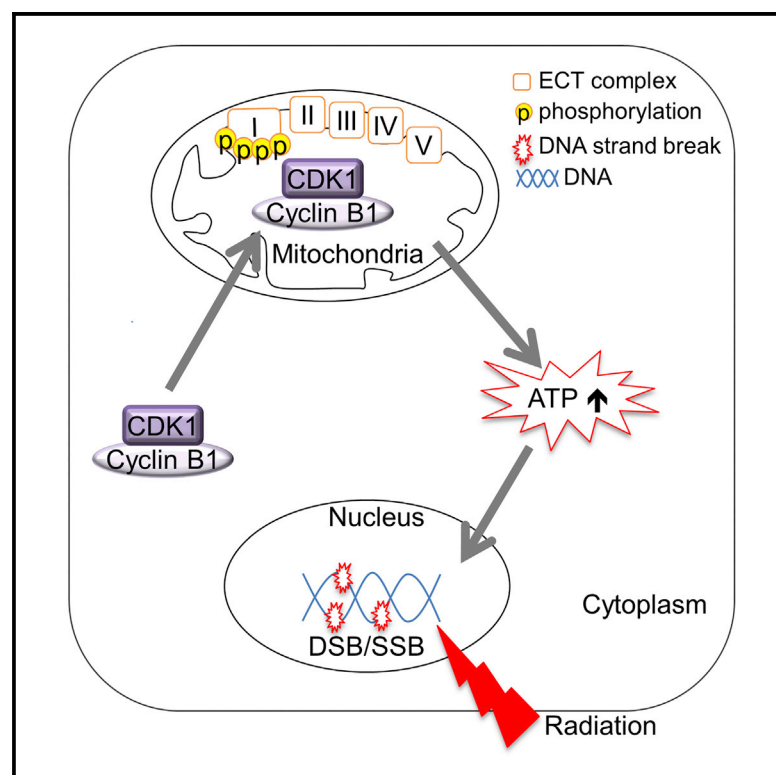# Cell Reports

CDK1 Enhances Mitochondrial Bioenergetics for Radiation-Induced DNA Repair

Graphical Abstract

Authors

Lili Qin, Ming Fan, Demet Candas, ...,
Gayle Woloschak, David J. Grdina,
Jian Jian Li

Correspondence

jijli@ucdavis.edu

In Brief

Qin et al. identify communication between mitochondrial bioenergetics and nuclear DNA repair. Upon radiation, the mitotic kinase CDK1 relocates to mitochondria and activates mitochondrial complex I. The resulting ATP generation is required for efficient DNA repair.

Highlights

- Oxygen consumption and mitochondrial ATP generation are enhanced in irradiated cells

- Upon radiation, CDK1 relocates to mitochondria

- Mitochondrial CDK1 boosts ATP generation via CI phosphorylation

- CDK1-regulated mitochondrial ATP generation favors DNA repair and cell survival

CrossMark

CellPress

CDK1 Enhances Mitochondrial Bioenergetics for Radiation-Induced DNA Repair

Lili Qin,[1] Ming Fan,[1] Demet Candas,[1] Guochun Jiang,[2] Stelios Papadopoulos,[3] Lin Tian,[3] Gayle Woloschak,[4] David J. Grdina,[5] and Jian Jian Li[1,*]

[1]Department of Radiation Oncology, National Cancer Institute-Designated Comprehensive Cancer Center, University of California Davis School of Medicine, Sacramento, CA 95817, USA
[2]Department of Medical Microbiology and Immunology, University of California Davis, Davis, CA 95616, USA
[3]Departments of Biochemistry and Molecular Medicine and Psychiatry and Behavioral Sciences, University of California Davis School of Medicine, Davis, CA 95616, USA
[4]Department of Radiation Oncology, Feinberg School of Medicine, Northwestern University, Chicago, IL 60611, USA
[5]Department of Radiation and Cellular Oncology, University of Chicago, Chicago, IL 60637, USA
*Correspondence: jjli@ucdavis.edu
http://dx.doi.org/10.1016/j.celrep.2015.11.015

SUMMARY

Nuclear DNA repair capacity is a critical determinant of cell fate under genotoxic stress conditions. DNA repair is a well-defined energy-consuming process. However, it is unclear how DNA repair is fueled and whether mitochondrial energy production contributes to nuclear DNA repair. Here, we report a dynamic enhancement of oxygen consumption and mitochondrial ATP generation in irradiated normal cells, paralleled with increased mitochondrial relocation of the cell-cycle kinase CDK1 and nuclear DNA repair. The basal and radiation-induced mitochondrial ATP generation is reduced significantly in cells harboring CDK1 phosphorylation-deficient mutant complex I subunits. Similarly, mitochondrial ATP generation and nuclear DNA repair are also compromised severely in cells harboring mitochondrially targeted, kinase-deficient CDK1. These results demonstrate a mechanism governing the communication between mitochondria and the nucleus by which CDK1 boosts mitochondrial bioenergetics to meet the increased cellular fuel demand for DNA repair and cell survival under genotoxic stress conditions.

INTRODUCTION

It is well known that radiation induces cell death because of nuclear DNA damage. To survive, cells need to maintain their genomic stability via checkpoint activation and a rapid DNA repair process. Lack of or an insufficient repair mechanism could lead to apoptosis or abnormal cell proliferation and cancer risk (Hoeijmakers, 2009; Kastan and Bartek, 2004). DNA repair has long been believed to be a highly energy-demanding process, consuming a large amount of cellular ATP (Bakkenist and Kastan, 2004; Hopfner et al., 2000; Paull and Gellert, 1999; Ward and Chen, 2004). As the powerhouse of mammalian cells, mito-

chondria provide the major cellular fuel for many critical processes in cell proliferation and survival (Pagliarini and Dixon, 2006; Scheibye-Knudsen et al., 2015). Inhibition of the respiration chain suppresses the spontaneous and H_2O_2-induced DNA damage repair in peripheral blood mononuclear cells (Gafter-Gvili et al., 2011). Mutations of mitochondrial genes encoding respiration chain subunits sensitize B-lymphoblastoid cells to radiation with decreased ATP generation and DNA repair gene expression (Kulkarni et al., 2011). However, the exact mechanism regulating mitochondrial bioenergetics to coordinate the nuclear DNA repair capacity under genotoxic stress conditions remains unknown.

Recent findings have revealed that Cyclin B1/CDK1, a well-defined cell-cycle kinase governing key steps of cell-cycle progression (Gautier et al., 1990; Hochegger et al., 2008), functions in the communication between mitochondrial activity and cell-cycle progression. CDK1 is involved in the integration of mitochondrial fission during G2/M transition through phosphorylation of mitochondrial fission proteins (Taguchi et al., 2007; Yamano and Youle, 2011). Cyclin B1/CDK1 has also been found to be able to phosphorylate and activate MnSOD and p53 in mitochondria to enhance cell survival (Candas et al., 2013; Nantajit et al., 2010). Recent data have also revealed that a fraction of mitochondrially relocated Cyclin B1/CDK1 can assist G2/M transition by boosting mitochondrial ATP generation via phosphorylation of mitochondrial respiration chain complex I (CI) subunits (Wang et al., 2014) and that CDK1-mediated Tom6 phosphorylation enhances the mitochondrial protein influx required for mitochondrial biogenesis and activity (Harbauer et al., 2014). Here we report that Cyclin B1/CDK1 mitochondrial relocation and mitochondrial ATP generation are enhanced in parallel with nuclear DNA repair in irradiated cells. Expression of CDK1 phosphorylation-deficient CI subunits or mitochondrially targeted kinase-deficient CDK1 inhibits radiation-induced mitochondrial ATP generation and DNA repair. These results provide evidence indicating communication between mitochondrial bioenergetics and nuclear DNA repair in which CDK1-mediated phosphorylation and activation of mitochondrial CI enhances mitochondrial ATP production to
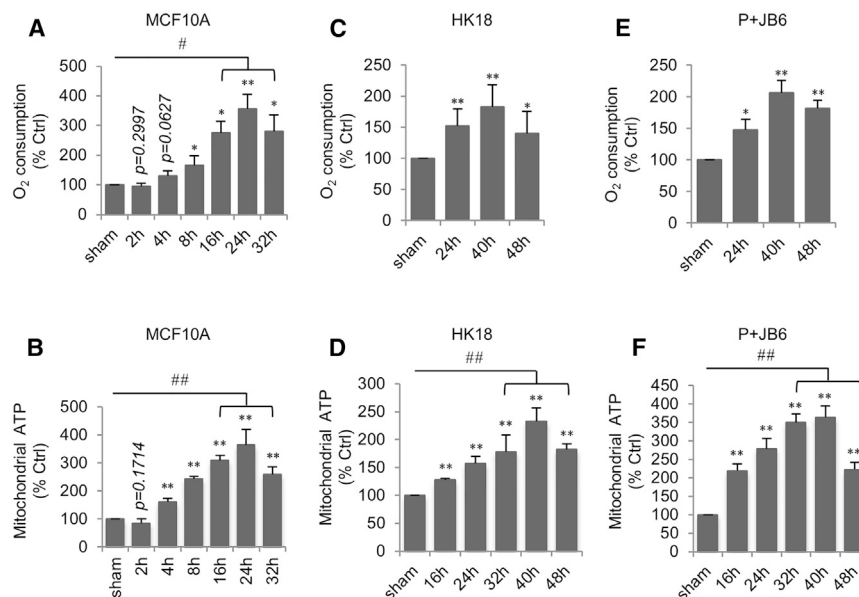
Figure 1. Radiation Enhances Mitochondrial ATP Generation and Oxygen Consumption

(A–F) Oxygen consumption (A, C, and E) and mitochondrial ATP generation (B, D, and F) were measured in MCF10A (A and B), HK18 (C and D), and P+JB6 (E and F) cells after 5-Gy radiation. Data represent mean ± S.E.M. *p < 0.05, **p < 0.01 irradiated cells versus non-irradiated sham control; #p < 0.05, ##p < 0.01 peak time versus non-irradiated sham control; n = 3.
See also Figure S1.

meet the increased energy demands for DNA damage repair and cell survival.

RESULTS

Radiation Enhances Mitochondrial Bioenergetics in Cells

We reported recently that the cell-cycle kinase CDK1 is involved in the control of mitochondrial bioenergetics to fuel G2/M transition in normal cell-cycle progression (Wang et al., 2014). In this study, we investigated whether CDK1-mediated mitochondrial bioenergetics contribute to the energy supply for nuclear DNA repair under genotoxic stress conditions. To this end, we first tested how mitochondrial respiration was altered after irradiation in three immortalized normal cell lines: human mammary epithelial MCF10A cells, human skin keratinocytes (HK18), and mouse skin epithelial P+JB6 cells. We found that, in all cell lines tested, mitochondrial ATP generation and oxygen consumption were enhanced significantly by radiation, although the peak values and times varied. In MCF10A cells, mitochondrial ATP generation showed a 3.63-fold increase, whereas oxygen consumption showed a 3.46-fold increase at the peak time of 24 hr post-radiation compared with a no-radiation sham control (Figures 1A and 1B). Meanwhile, mitochondrial superoxide levels were found to be increased, paralleled with a slight increase in MnSOD activity in irradiated MCF10A cells (Figures S1A and S1B). Enhanced mitochondrial ATP generation and oxygen consumption were also observed in the HK18 (Figures 1C and 1D) and p+JB6 (Figures 1E and 1F) cell lines, with a peak time around 40 hr post-radiation, indicating that the induction of mitochondrial respiration by radiation is not cell-type specific (MCF10A cells were used in subsequent experiments). Overall, these data demonstrate that mitochondrial bioenergetics are enhanced by a single dose of ionizing radiation in normal cells.

Radiation-Induced DNA Damage Repair Links to Mitochondrial Bioenergetics

Because repair of radiation-induced DNA damage is essential for cell survival and maintenance of genomic stability, and DNA repair is an ATP-consuming process, we hypothesized that the irradiated cells enhance their mitochondrial ATP generation to meet the increased energy demand for nuclear DNA repair. We first determined the levels of γH2A.X, a marker of DNA double-strand breaks (DSBs), which was increased 2 hr post-radiation and then decreased gradually (Figure 2A). γH2A.X foci formation in irradiated cells can be detected as early as 15 min, with 100% cells showing nuclear γH2A.X focus formation (Figure S2A), which remained constant until 2 hr (Figure 2B; Figure S2A). The number of γH2A.X focus-containing cells decreased gradually from 4 hr post-radiation (Figure 2B; Figure S2A). Comet assay data displayed a similar DNA repair pattern, shown by tail DNA intensity and tail moment in irradiated cells (Figures 3C and 3D).

Next we examined the involvement of non-homologous end joining (NHEJ) and homologous recombination (HR) in DNA DSB repair. The NHEJ pathway was found to be activated early post-radiation, as indicated by 53BP1 focus formation (Figure 2E; Figure S2B) and increased DNA-dependent protein kinase, catalytic subunit (DNA-PKcs) phosphorylation, along with a constant level of Ku70/80 (Figure 2A). In contrast, HR repair was evidently increased 24 hr post-radiation, as measured by Rad51 focus formation (Figure 2F), without the apparent enhancement of Rad51 protein levels (Figure 2A). These data demonstrate a possibility that, although both the NHEJ and HR repair pathways are involved in irradiated cells, only HR repair coincides with radiation-enhanced mitochondrial ATP generation in terms of timing, which needs to be investigated further.

Radiation-induced G2/M arrest is believed to help cells with DNA damage repair, and cells with unrepaired lesions undergo apoptosis or tumorigenesis (Hoeijmakers, 2009; Kastan and Bartek, 2004). Our data show that the percentage of cells in G2/M phase was increased significantly 2–8 hr after radiation (Figure S2C), with a relative small fraction of apoptotic cells detected during the same period of time (Figures S2D and S2E).
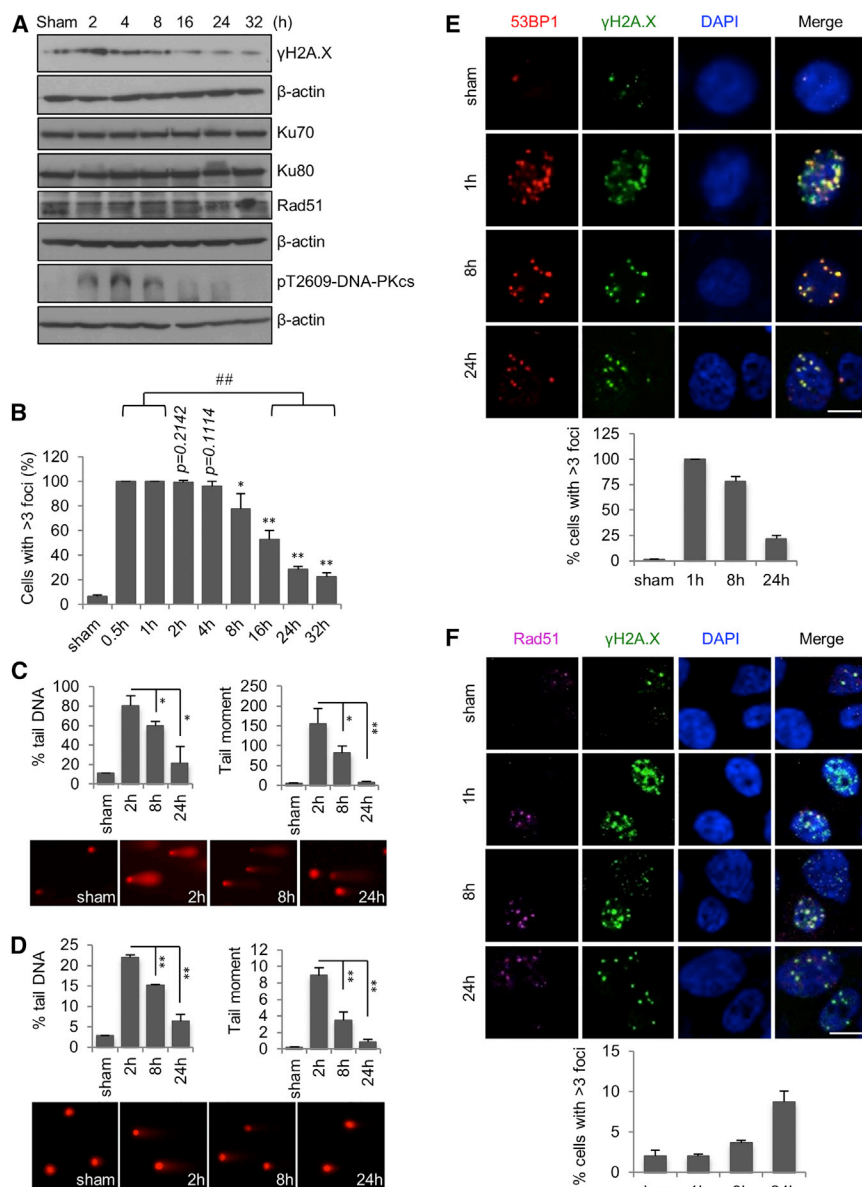
Figure 2. Nuclear DNA Repair Capacity Is Paralleled with Mitochondrial ATP Generation

(A) Western blot analysis of radiation-induced DNA damage repair.

(B) Percentage of cells with >3 nuclear γH2A.X foci at different time intervals after 5-Gy radiation. Data represent mean ± SEM. *p < 0.05, **p < 0.01, n = 3; ##p < 0.01; n = 3. See also Figure S2A.

(C) Alkaline comet assay of DNA damage. Data represent mean ± SEM. *p < 0.05, **p < 0.01. Bottom: representative images of tailed DNA. Magnification, 20×.

(D) Neutral comet assay of DNA damage. Data represent mean ± SEM. **p < 0.01. Bottom: representative images of tailed DNA. Magnification, 20×.

(E) 53BP1 focus formation representing NHEJ repair of radiation-induced DNA DSBs. Scale bar, 10 μm. See also Figure S2B.

(F) Rad51 focus formation representing HR repair of radiation-induced DNA DSBs. Scale bar, 10 μm.

16 hr post-radiation (Figure 3A), when mitochondrial ATP generation reached its peak time (Figure 1B) and most of the damaged DNA had been repaired (Figure 2B). Taken together, as summarized in Figure 3B and Figure S3A, the enhanced CDK1 mitochondrial relocation is coordinated with increased mitochondrial bioenergetics and DNA repair in irradiated cells. Notably, pT161-CDK1 (active phosphorylated CDK1) levels in both total cell lysates and mitochondrial fractions were increased by radiation around 2 hr and remained high throughout the experiment (Figure 3A; Figure S3B; the purity of the mitochondrial preparation is shown in Figure S3C). In contrast to the enhanced mitochondrial CDK1 and Cyclin B1, total cellular CDK1 and Cyclin B1 protein remained unchanged or increased slightly within 32 hr of testing (Figure S3B). CDK1 mitochondrial relocation was further confirmed by electron microscopy (Figure S3D) and immunostaining (Figure S3E). Inhibition of Cyclin B1 expression using small interfering RNA (siRNA) knockdown significantly decreased the mitochondrial CDK1 level and vice versa (Figure 3C), suggesting the possibility that both proteins relocate to mitochondria together. In addition, radiation-induced mitochondrial relocation of Cyclin B1 and CDK1 appeared not to be dose-dependent (Figure S3F).

We then tested whether CDK1-mediated CI activation contributes to radiation-enhanced mitochondrial ATP generation and DNA repair. As shown in Figure 3D, both basal and radiation-induced mitochondrial ATP were reduced significantly in cells harboring CDK1 phosphorylation-deficient CI subunits compared with the empty vector control cells, and, moreover,

Radiation-Induced Mitochondrial Relocation of Cyclin B1 and CDK1

Our previous study demonstrated that radiation enhances mitochondrial relocation of Cyclin B1 and CDK1 in multiple normal and cancer cell lines (Candas et al., 2013; Nantajit et al., 2010) and that mitochondrially relocated CDK1 phosphorylates CI subunits and, consequently, upregulates CI activity and mitochondrial ATP generation during G2/M transition (Wang et al., 2014). We then wondered whether CDK1-enhanced mitochondrial ATP generation is required for nuclear DNA repair and cell survival under genotoxic conditions. We found that the first detectable increase in the mitochondrial relocation of Cyclin B1 and CDK1 appeared at 4 hr (Figure 3A), when mitochondrial ATP production started to increase (Figure 1B) and DNA repair activity was detectable (Figure 2B), and both peaked around
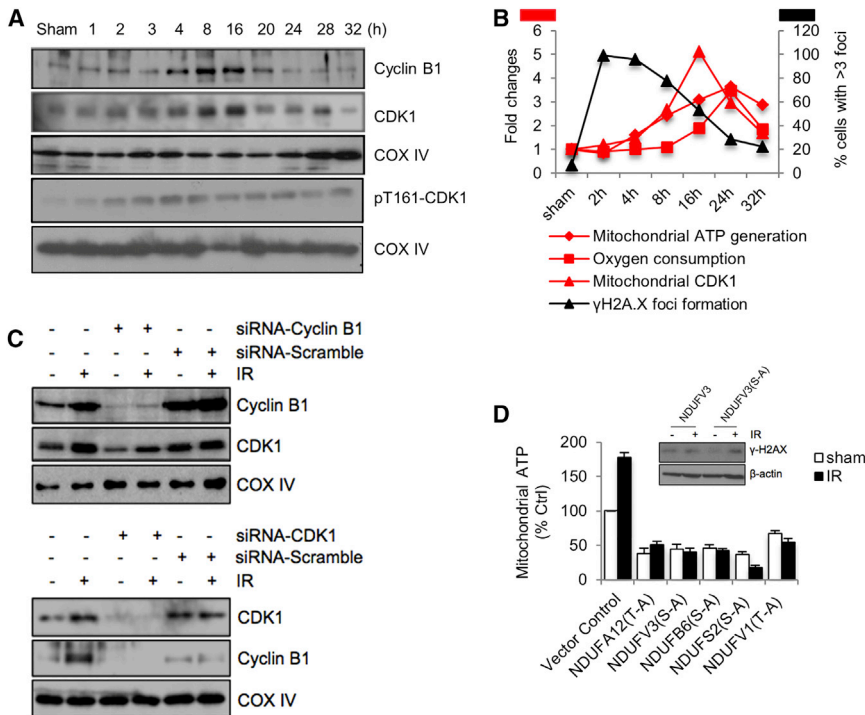
Figure 3. Mitochondrial CDK1-Mediated Phosphorylation of CI Subunits Contributes to Radiation-Enhanced Mitochondrial ATP Generation

(A) Western blot of enhanced mitochondrial relocation of Cyclin B1 and CDK1 in irradiated cells. COXIV, mitochondria loading control. See also Figure S3.

(B) Summary of coordinated Cyclin B1/CDK1 mitochondrial relocation with enhanced mitochondrial respiration and DNA repair. Left y axis: fold changes in mitochondrial ATP generation, oxygen consumption, and levels of mitochondrially relocated CDK1. Right y axis: percentage of cells with >3 nuclear γH2A.X foci. See also Figure S3A.

(C) Cells were transfected with Cyclin B1 (top) or CDK1 (bottom) siRNA for 24 hr and irradiated with 5 Gy followed by western blotting of mitochondrial fractions 24 hr after radiation. IR, ionizing radiation.

(D) Cells were transfected with each of the CDK1 phosphorylation-deficient mutant CI subunits for 24 hr and irradiated with 5 Gy, followed by measurement of mitochondrial ATP generation 24 hr post-radiation (n = 3). Inset: γH2A.X expression levels measured in irradiated cells transfected with the wild-type or phosphorylation-deficient mutant NDUFV3 subunit.

these mutant CI subunit-harboring cells did not show any radiation-enhanced mitochondrial ATP. In addition, γH2A.X protein levels were increased significantly in irradiated NDUFV3(S-A)-harboring cells 24 hr post-radiation but not in irradiated NDUFV3wt-harboring cells (Figure 3D, inset; the expression of GFP-tagged NDUFV3 is shown in Figure S3G). These data indicate that CDK1-mediated phosphorylation of mitochondrial CI subunits is associated with radiation-enhanced mitochondrial ATP generation and DNA repair.

Mitochondrially Targeted Expression of Kinase-Deficient CDK1 Compromises Radiation-Enhanced Mitochondrial Bioenergetics and Inhibits DNA Repair

To further investigate whether mitochondrial CDK1 kinase activity is required for radiation-enhanced mitochondrial bioenergetics and DNA repair, we transfected MCF10A cells with mitochondrially targeted Cyclin B1 together with kinase-deficient mutant CDK1 (MTS-CDK1-dn) and measured mitochondrial ATP generation and DNA repair. Schematics of the DNA constructs for knockdown of mitochondrially active CDK1 and the co-expression of fluorescence-tagged Cyclin B1 (GFP) and CDK1 (red fluorescent protein [RFP]) in transfected cells are shown in Figures S4A and S4B. With a mitochondrial targeting sequence (MTS) cloned in-frame upstream of Cyclin B1 and CDK1 cDNA, expression of Cyclin B1 and CDK1 can be executed specifically in the mitochondria to avoid disturbing their functions in the nucleus and cytosol. Radiation-induced mitochondrial ATP (Figure 4A) and superoxide (Figure S4C) were compromised significantly in MTS-CDK1-dn cells compared with empty vector control cells. Likewise, an elevated γH2A.X protein level (Figure 4B) and increased γH2A.X focus-

containing cells (Figure 4C) were detected in irradiated MTS-CDK1-dn cells. Furthermore, clonogenic survival was reduced by about 25% in irradiated cells harboring MTS-CDK1-dn compared with empty vector control cells (Figure 4D). Together, these results suggest that kinase-active mitochondrial CDK1 contributes to radiation-enhanced mitochondrial ATP generation to meet the increased cellular energy demands for DNA repair in irradiated cells.

DISCUSSION

Here we report a mechanism by which CDK1 coordinates mitochondrial ATP generation with radiation-induced nuclear DNA damage repair (Figure 4E). We show that mitochondrial ATP generation is increased in irradiated cells in a time-dependent manner, paralleled with radiation-induced nuclear DNA damage and mitochondrial accumulation of Cyclin B1/CDK1. Mitochondrially targeted knockdown of CDK1 as well as expression of CDK1 phosphorylation-deficient subunits of CI severely compromises enhanced mitochondrial ATP generation and inhibits DNA repair in irradiated cells.

Timely and efficient DNA repair is a critical step for cells to survive genotoxic stress such as ionizing radiation (Hoeijmakers, 2009), which requires consumption of cellular energy (Bakkenist and Kastan, 2004; Kulkarni et al., 2011; Ward and Chen, 2004). As the major contributor of cellular energy production by generating ATP (Pagliarini and Dixon, 2006; Scheibye-Knudsen et al., 2015), mitochondrially derived ATP is enhanced under oxidative stress conditions such as radiation (Jin et al., 2015; Lu et al., 2015). Besides this, whether or how mitochondrial bioenergetics affect the DNA damage repair capacity of cells under radiation
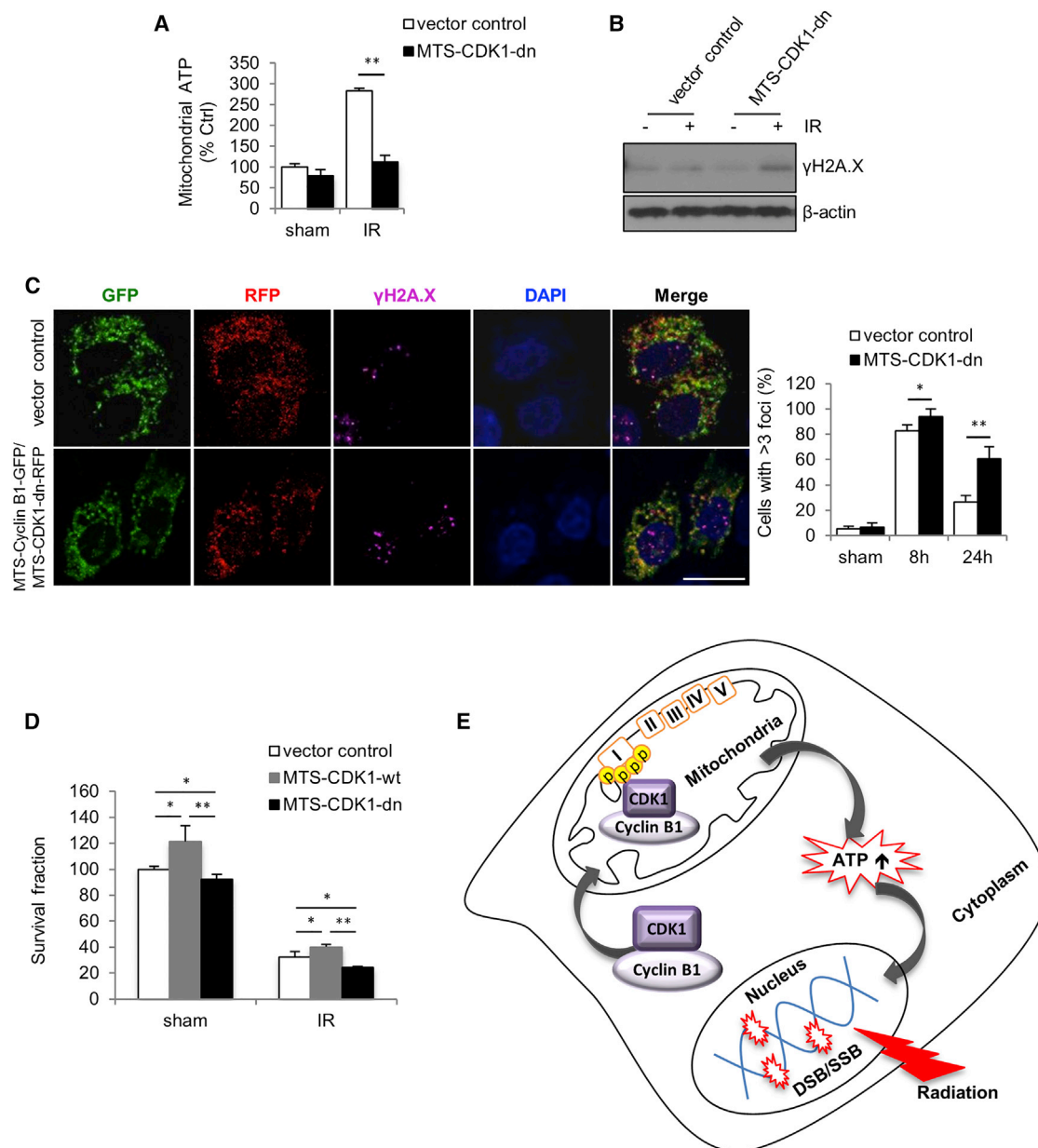
Figure 4. Mitochondrially Targeted, Kinase-Deficient CDK1 Compromises Enhanced Mitochondrial Bioenergetics and Inhibits DNA Repair

(A–C) Mitochondrial ATP generation (A), γH2A.X protein levels (B), and γH2A.X focus formation (scale bar, 20 μm) (C) were measured in mitochondrially targeted, kinase-deficient CDK1-harboring cells and empty vector control cells. In (A), data represent mean ± SEM. **p < 0.01, n = 3. In (C), right, data represent mean ± SEM. *p < 0.05, **p < 0.01, n = 3.

(D) Clonogenic survival of cells harboring mitochondrially targeted wild-type or kinase-deficient mutant CDK1 and empty vector control cells under 5-Gy radiation. Data represent mean ± SEM. *p < 0.05, **p < 0.01, n = 3.

(E) A proposed function of CDK1 in coordinating mitochondrial bioenergetics with nuclear DNA repair in irradiated cells. Mitochondrial relocation of CDK1 is enhanced by radiation, which subsequently upregulates mitochondrial ATP generation via phosphorylation of CI subunits to meet the increased cellular fuel demand for DNA repair.

stress has not been defined. Single-nucleotide mutations in mitochondrial genes involved in ATP synthesis result in an increased number of chromosomal aberrations and decreased mitotic indices following acute radiation exposure in human lymphoblastoid cells (Kulkarni et al., 2009), suggesting that mito-

chondrial ATP generation is linked with DNA repair. In irradiated Jurkat cells, cellular ATP levels decrease continuously under oligomycin-containing, glucose-free medium culture conditions but not under glucose-free-only medium or oligomycin-containing regular medium culture conditions (Eguchi et al., 1997),

indicating that, in normal cells, mitochondrial oxidative phosphorylation and glycolysis might complement each other to maintain an efficient energy supply. Similar to normal cells, tumor cells also show radiation-enhanced mitochondrial respiration (Gong et al., 1998; Lu et al., 2015; Meike et al., 2011; Yamamori et al., 2012), and increased cellular ATP generation accompanied by reduced DNA damage leads to radioresistance (Artesi et al., 2015). Our results, together with these reported findings, indicate a previously unknown communication between mitochondrial bioenergetics and nuclear DNA repair through which cells enhance the mitochondrial energy metabolism to meet the increased fuel demand to recover from DNA damages.

It should be noticed that, although both the NHEJ and HR pathways are shown to be involved in DNA repair following irradiation, HR repair seems to be more dependent on mitochondrial ATP supplies, indicating a possibility that the HR pathway accounts for the decreased cell survival observed in cells harboring kinase-deficient CDK1. Further investigations are needed to elucidate whether a specific DNA repair pathway requires mitochondrial bioenergetics and whether such a dynamic communication between mitochondrial bioenergetics and nuclear DNA repair is also activated in cancer cells.

Ionizing radiation is a potent inducer of apoptosis in many different cell types (Shao et al., 2014), which is also an ATP/energy-demanding process, and the pertinent deployment of energy between DNA repair and apoptosis will potentially determine cell fate (Bernstein et al., 2002). A study in Jurkat cells has suggested that both glycolysis and mitochondrial oxidative phosphorylation could be the energy support of apoptosis (Eguchi et al., 1997). Although, in this study, apoptosis of irradiated cells was found to be increased gradually in the phase of mitochondrial energy enhancement, radiation-induced apoptosis in MCF10A cells was not affected by the expression of mitochondrially targeted, kinase-deficient CDK1 (Candas et al., 2013), suggesting that CDK1/CI-mediated mitochondrial bioenergetics are probably not required for radiation-induced apoptosis in normal cells.

Under genotoxic conditions, a specific group of stress-responsive proteins, including MnSOD, p53, Cyclin B1/CDK1, Cyclin D1/CDK4, and survivin (Horbinski and Chu, 2005; Jin et al., 2015; Lu et al., 2015; Nantajit et al., 2010; Pagliarini and Dixon, 2006), are inflexed to mitochondria to induce cellular adaptive protection. As a well-defined cell-cycle G2/M transition regulator, the precise subcellular relocation of Cyclin B1/CDK1 is required for the regulation of cell-cycle progression (Gavet and Pines, 2010). Recently, CDK1 has been found to relocate to mitochondria to coordinate energy metabolism with increased fuel demand for cell-cycle G2/M transition (Wang et al., 2014). Interestingly, as the major entry point of electrons into the respiration chain, CI has been identified to be a substrate of CDK1 during cell-cycle progression (Dephoure et al., 2008; Wang et al., 2014). These findings, together with our data showing that kinase-deficient CDK1 and CDK1 phosphorylation-deficient CI subunits can inhibit radiation-enhanced mitochondrial ATP generation and DNA repair, support the concept that CDK1-mediated activation of the mitochondrial respiration chain coordinates nuclear DNA repair with increased cellular energy supply.

In conclusion, our data demonstrate a pathway through which mitochondrially relocated CDK1 phosphorylates multiple CI subunits, boosting mitochondrial ATP generation to meet the increased energy demand for DNA repair and cell survival. This is a unique cross-talk between mitochondrial energy metabolism and nuclear DNA repair that may contribute to further our understanding of how cell fate was decided under genotoxic stress conditions.

EXPERIMENTAL PROCEDURES

Cell Culture and Treatment

MCF-10A cells were maintained as described previously (Soule et al., 1990). P+JB6 cells were maintained in minimum essential medium (MEM) supplemented with 5% fetal bovine serum (FBS), and HK18 cells were maintained in DMEM supplemented with 10% FBS. Exponentially grown cells were irradiated with a cabinet X-ray system, Faxitron series, at a dose rate of 1.382 Gy/min. See the Supplemental Experimental Procedures for details.

Western Blotting

For each assay, 20 μg of protein was separated on an SDS-PAGE gel and transferred to a polyvinylidene difluoride (PVDF) membrane, followed by blocking of the membrane in 5% fat-free milk for 1 hr. The membrane was then incubated with primary antibodies (refer to the Supplemental Experimental Procedures for details) at 4°C overnight, followed by incubation with secondary antibodies for 1 hr at room temperature. Signals were then detected with an enhanced chemiluminescence (ECL) detection kit.

Measurement of Mitochondrial ATP Production

Mitochondrial ATP production was measured following a published method (Vives-Bauza et al., 2007) with modifications. See the Supplemental Experimental Procedures for details.

Measurement of Oxygen Consumption

Exponentially growing cells ($1-2 \times 10^6$) were harvested and resuspended in 300 μl of oxygen consumption buffer (25 mM sucrose, 15 mM KCl, 1 mM EGTA, 0.5 mM $MgCl_2$, and 30 mM K_2HPO_4). Oxygen consumption was monitored at 30°C with succinate as the complex II substrate using Clarke-type oxygen electrode (Rank Brothers) following the manufacturer's instructions.

Comet Assay

Alkaline and neutral comet assays were performed following the manufacturer's instructions (Trevigen Laboratory). DNA was stained with propidium iodide, and images of the comets were captured under a fluorescence microscope. For each sample, a minimum of 50 cells was analyzed using the software CASPlab, and the DNA damage was represented as percent tail DNA and tail moment. The experiments were repeated twice, and control (untreated cells) were used to determine the characteristics of data for a healthy cell.

Focus Formation Assay

Cells growing on coverslips were fixed in 4% paraformaldehyde for 10 min at room temperature, permeabilized in 0.2% Triton X-100 for 10 min, and blocked in 1% BSA for 1 hr at room temperature. Cells were then incubated with the indicated primary antibodies overnight at 4°C, followed by incubation with the fluorescence-conjugated secondary antibody for 1 hr in the dark at room temperature. Nuclei were counterstained with DAPI contained in mounting solution. Images were acquired using a Zeiss LSM710 confocal microscope system and analyzed with ImageJ software. The experiment was repeated three times, and at least 100 cells were scored for each sample. Data represent the percentage of cells containing more than three foci.

Preparation of Mitochondrial Fractions from Cultured Cells

Mitochondrial and cytosolic fractions were prepared as described previously (Frezza et al., 2007) with modifications. Briefly, cells were homogenized using a Teflon pestle in ice-cold isolation buffer for cells (IBc). The homogenates

were centrifuged at 600 × g for 10 min at 4°C, and the supernatants were collected and centrifuged further at 7,000 × g for 10 min at 4°C. The supernatants were transferred to new tubes as the cytosolic fractions, and the pellets were washed with ice-cold IBc buffer twice and re-suspended in cell lysis buffer as mitochondrial fractions.

Plasmid Constructs and Cell Transfection
Cyclin B1, CDK1, and CI subunits DNA constructs have been established previously by our lab (Wang et al., 2014). Exponentially growing cells were transfected using METAFECTENE-PRO following the manufacturer's instructions.

Gene Silencing by siRNA
siRNAs targeting Cyclin B1 and CDK1 mRNA were synthesized using the Silencer siRNA construction kit (Ambion) and transfected to cells using Lipofectamine RNAi MAX (Invitrogen). See the Supplemental Experimental Procedures for details.

Clonogenic Survival Assay
Cells transfected with mitochondrion-targeting wild-type or kinase-deficient mutant CDK1 were irradiated 24 hr after transfection and seeded in 60-mm plates with three different cell numbers in triplicate. Colonies were stained on day 7 with Coomassie blue dye and counted. The clonogenic survival ability of irradiated cells was represented as the survival fraction normalized to that of no-radiation control cells transfected with empty vector.

Statistical Analysis
Data are presented as mean ± SEM from at least three independent experiments. Statistical analysis was performed with unpaired two-tailed Student's t test. $p < 0.05$ was considered statistically significant.

SUPPLEMENTAL INFORMATION

Supplemental Information includes Supplemental Experimental Procedures and four figures and can be found with this article online at http://dx.doi.org/10.1016/j.celrep.2015.11.015.

AUTHOR CONTRIBUTIONS

L.Q. and J.J.L. designed the study. L.Q., M.F., and D.C. performed the experiments. S.P. and L.T. provided technical assistance. L.Q., D.C., G.J., and J.J.L. wrote the manuscript.

ACKNOWLEDGMENTS

REFERENCES

Artesi, M., Kroonen, J., Bredel, M., Nguyen-Khac, M., Deprez, M., Schoysman, L., Poulet, C., Chakravarti, A., Kim, H., Scholtens, D., et al. (2015). Connexin 30 expression inhibits growth of human malignant gliomas but protects them against radiation therapy. Neuro-oncol. *17*, 392–406.

Bakkenist, C.J., and Kastan, M.B. (2004). Initiating cellular stress responses. Cell *118*, 9–17.

Bernstein, C., Bernstein, H., Payne, C.M., and Garewal, H. (2002). DNA repair/pro-apoptotic dual-role proteins in five major DNA repair pathways: fail-safe protection against carcinogenesis. Mutat. Res. *511*, 145–178.

Candas, D., Fan, M., Nantajit, D., Vaughan, A.T., Murley, J.S., Woloschak, G.E., Grdina, D.J., and Li, J.J. (2013). CyclinB1/Cdk1 phosphorylates mitochondrial antioxidant MnSOD in cell adaptive response to radiation stress. J. Mol. Cell Biol. *5*, 166–175.

Dephoure, N., Zhou, C., Villén, J., Beausoleil, S.A., Bakalarski, C.E., Elledge, S.J., and Gygi, S.P. (2008). A quantitative atlas of mitotic phosphorylation. Proc. Natl. Acad. Sci. USA *105*, 10762–10767.

Eguchi, Y., Shimizu, S., and Tsujimoto, Y. (1997). Intracellular ATP levels determine cell death fate by apoptosis or necrosis. Cancer Res. *57*, 1835–1840.

Frezza, C., Cipolat, S., and Scorrano, L. (2007). Organelle isolation: functional mitochondria from mouse liver, muscle and cultured fibroblasts. Nat. Protoc. *2*, 287–295.

Gafter-Gvili, A., Herman, M., Ori, Y., Korzets, A., Chagnac, A., Zingerman, B., Rozen-Zvi, B., Gafter, U., and Malachi, T. (2011). Inhibition of mitochondrial function reduces DNA repair in human mononuclear cells. Leuk. Res. *35*, 219–225.

Gautier, J., Minshull, J., Lohka, M., Glotzer, M., Hunt, T., and Maller, J.L. (1990). Cyclin is a component of maturation-promoting factor from Xenopus. Cell *60*, 487–494.

Gavet, O., and Pines, J. (2010). Activation of cyclin B1-Cdk1 synchronizes events in the nucleus and the cytoplasm at mitosis. J. Cell Biol. *189*, 247–259.

Gong, B., Chen, Q., and Almasan, A. (1998). Ionizing radiation stimulates mitochondrial gene expression and activity. Radiat. Res. *150*, 505–512.

Harbauer, A.B., Opalińska, M., Gerbeth, C., Herman, J.S., Rao, S., Schönfisch, B., Guiard, B., Schmidt, O., Pfanner, N., and Meisinger, C. (2014). Mitochondria. Cell cycle-dependent regulation of mitochondrial preprotein translocase. Science *346*, 1109–1113.

Hochegger, H., Takeda, S., and Hunt, T. (2008). Cyclin-dependent kinases and cell-cycle transitions: does one fit all? Nat. Rev. Mol. Cell Biol. *9*, 910–916.

Hoeijmakers, J.H. (2009). DNA damage, aging, and cancer. N. Engl. J. Med. *361*, 1475–1485.

Hopfner, K.P., Karcher, A., Shin, D.S., Craig, L., Arthur, L.M., Carney, J.P., and Tainer, J.A. (2000). Structural biology of Rad50 ATPase: ATP-driven conformational control in DNA double-strand break repair and the ABC-ATPase superfamily. Cell *101*, 789–800.

Horbinski, C., and Chu, C.T. (2005). Kinase signaling cascades in the mitochondrion: a matter of life or death. Free Radic. Biol. Med. *38*, 2–11.

Jin, C., Qin, L., Shi, Y., Candas, D., Fan, M., Lu, C.L., Vaughan, A.T., Shen, R., Wu, L.S., Liu, R., et al. (2015). CDK4-mediated MnSOD activation and mitochondrial homeostasis in radioadaptive protection. Free Radic. Biol. Med. *81*, 77–87.

Kastan, M.B., and Bartek, J. (2004). Cell-cycle checkpoints and cancer. Nature *432*, 316–323.

Kulkarni, R., Reither, A., Thomas, R.A., and Tucker, J.D. (2009). Mitochondrial mutant cells are hypersensitive to ionizing radiation, phleomycin and mitomycin C. Mutat. Res. *663*, 46–51.

Kulkarni, R., Thomas, R.A., and Tucker, J.D. (2011). Expression of DNA repair and apoptosis genes in mitochondrial mutant and normal cells following exposure to ionizing radiation. Environ. Mol. Mutagen. *52*, 229–237.

Lu, C.L., Qin, L., Liu, H.C., Candas, D., Fan, M., and Li, J.J. (2015). Tumor cells switch to mitochondrial oxidative phosphorylation under radiation via mTOR-mediated hexokinase II inhibition–a Warburg-reversing effect. PLoS ONE *10*, e0121046.

Meike, S., Yamamori, T., Yasui, H., Eitaki, M., Matsuda, A., and Inanami, O. (2011). 8-Aminoadenosine enhances radiation-induced cell death in human lung carcinoma A549 cells. J. Radiat. Res. (Tokyo) *52*, 456–463.

Nantajit, D., Fan, M., Duru, N., Wen, Y., Reed, J.C., and Li, J.J. (2010). Cyclin B1/Cdk1 phosphorylation of mitochondrial p53 induces anti-apoptotic response. PLoS ONE *5*, e12341.

Pagliarini, D.J., and Dixon, J.E. (2006). Mitochondrial modulation: reversible phosphorylation takes center stage? Trends Biochem. Sci. *31*, 26–34.

Paull, T.T., and Gellert, M. (1999). Nbs1 potentiates ATP-driven DNA unwinding and endonuclease cleavage by the Mre11/Rad50 complex. Genes Dev. *13*, 1276–1288.

Scheibye-Knudsen, M., Fang, E.F., Croteau, D.L., Wilson, D.M., 3rd, and Bohr, V.A. (2015). Protecting the mitochondrial powerhouse. Trends Cell Biol. *25*, 158–170.

Shao, L., Luo, Y., and Zhou, D. (2014). Hematopoietic stem cell injury induced by ionizing radiation. Antioxid. Redox Signal. *20*, 1447–1462.

Soule, H.D., Maloney, T.M., Wolman, S.R., Peterson, W.D., Jr., Brenz, R., McGrath, C.M., Russo, J., Pauley, R.J., Jones, R.F., and Brooks, S.C. (1990). Isolation and characterization of a spontaneously immortalized human breast epithelial cell line, MCF-10. Cancer Res. *50*, 6075–6086.

Taguchi, N., Ishihara, N., Jofuku, A., Oka, T., and Mihara, K. (2007). Mitotic phosphorylation of dynamin-related GTPase Drp1 participates in mitochondrial fission. J. Biol. Chem. *282*, 11521–11529.

Vives-Bauza, C., Yang, L., and Manfredi, G. (2007). Assay of mitochondrial ATP synthesis in animal cells and tissues. Methods Cell Biol. *80*, 155–171.

Wang, Z., Fan, M., Candas, D., Zhang, T.Q., Qin, L., Eldridge, A., Wachsmann-Hogiu, S., Ahmed, K.M., Chromy, B.A., Nantajit, D., et al. (2014). Cyclin B1/Cdk1 coordinates mitochondrial respiration for cell-cycle G2/M progression. Dev. Cell *29*, 217–232.

Ward, I., and Chen, J. (2004). Early events in the DNA damage response. Curr. Top. Dev. Biol. *63*, 1–35.

Yamamori, T., Yasui, H., Yamazumi, M., Wada, Y., Nakamura, Y., Nakamura, H., and Inanami, O. (2012). Ionizing radiation induces mitochondrial reactive oxygen species production accompanied by upregulation of mitochondrial electron transport chain function and mitochondrial content under control of the cell cycle checkpoint. Free Radic. Biol. Med. *53*, 260–270.

Yamano, K., and Youle, R.J. (2011). Coupling mitochondrial and cell division. Nat. Cell Biol. *13*, 1026–1027.

CDK1 Enhances Mitochondrial Bioenergetics

for Radiation-Induced DNA Repair

Lili Qin, Ming Fan, Demet Candas, Guochun Jiang, Stelios Papadopoulos, Lin Tian, Gayle Woloschak, David J. Grdina, and Jian Jian Li
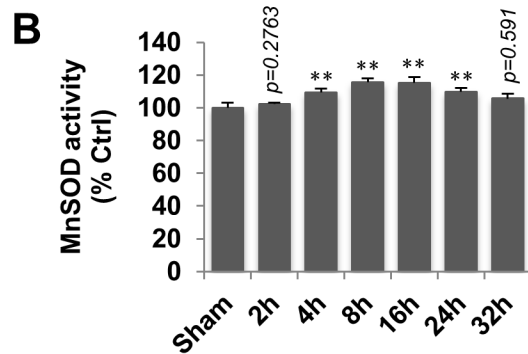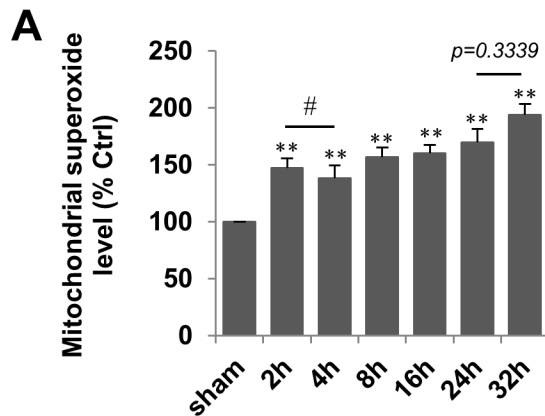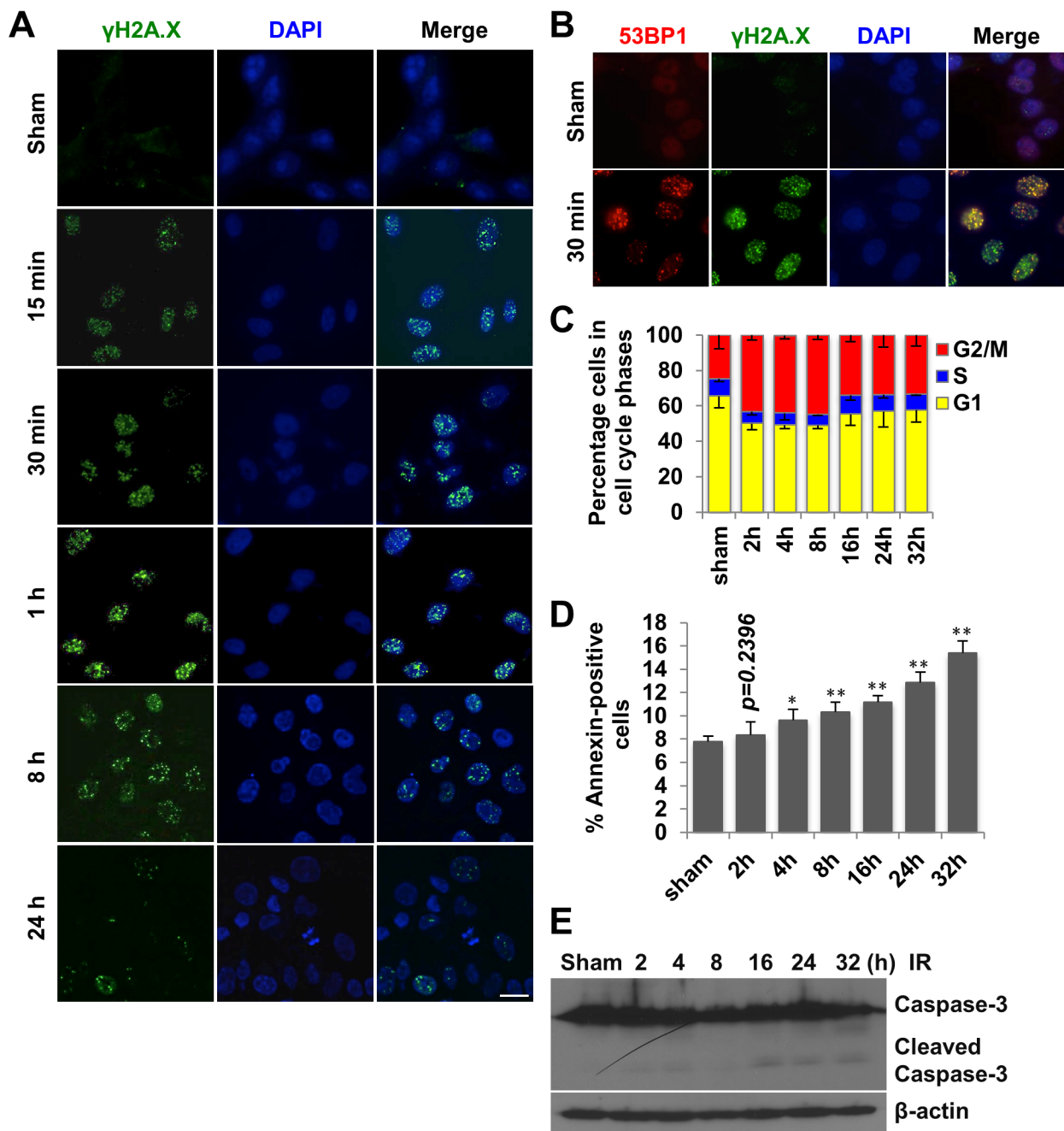
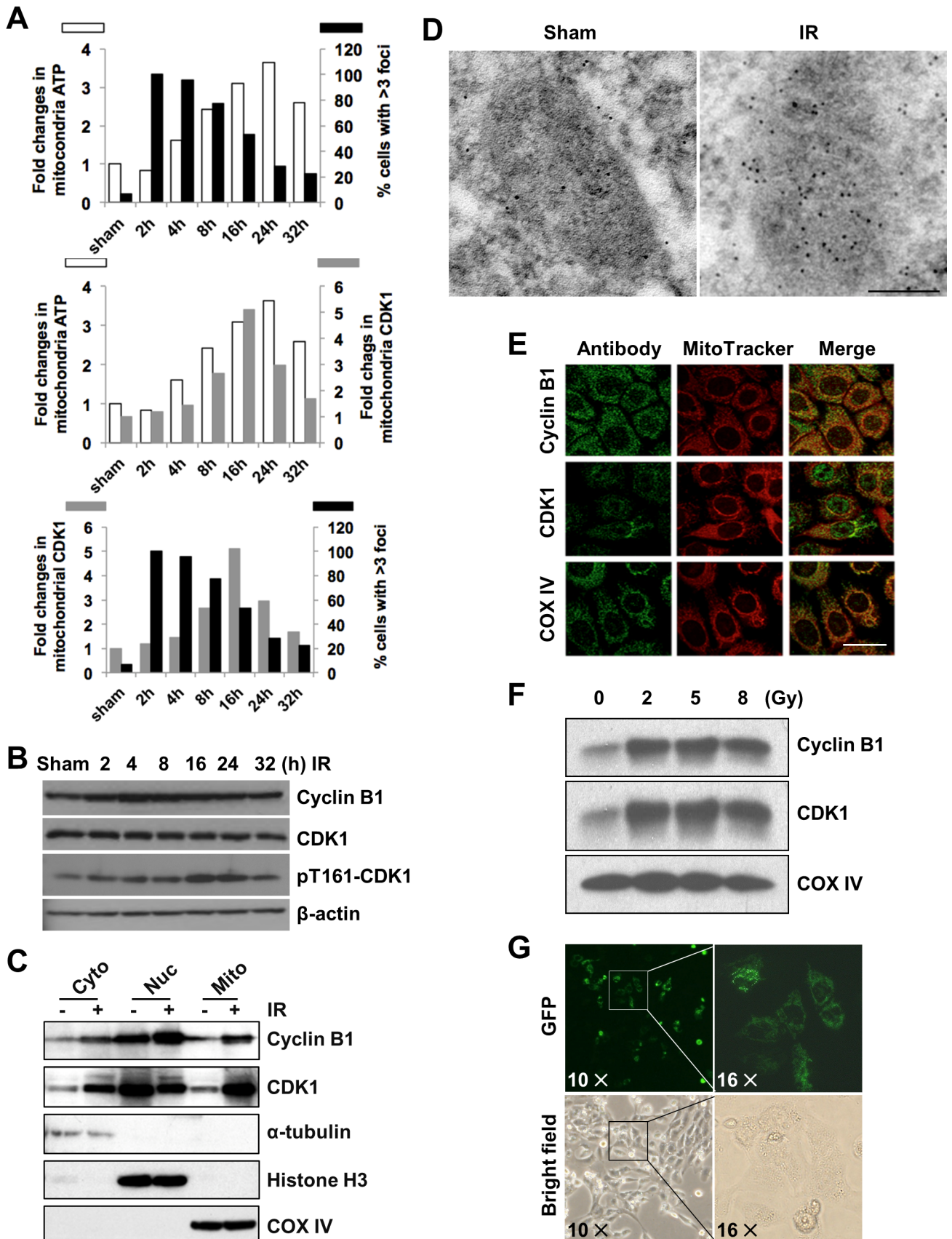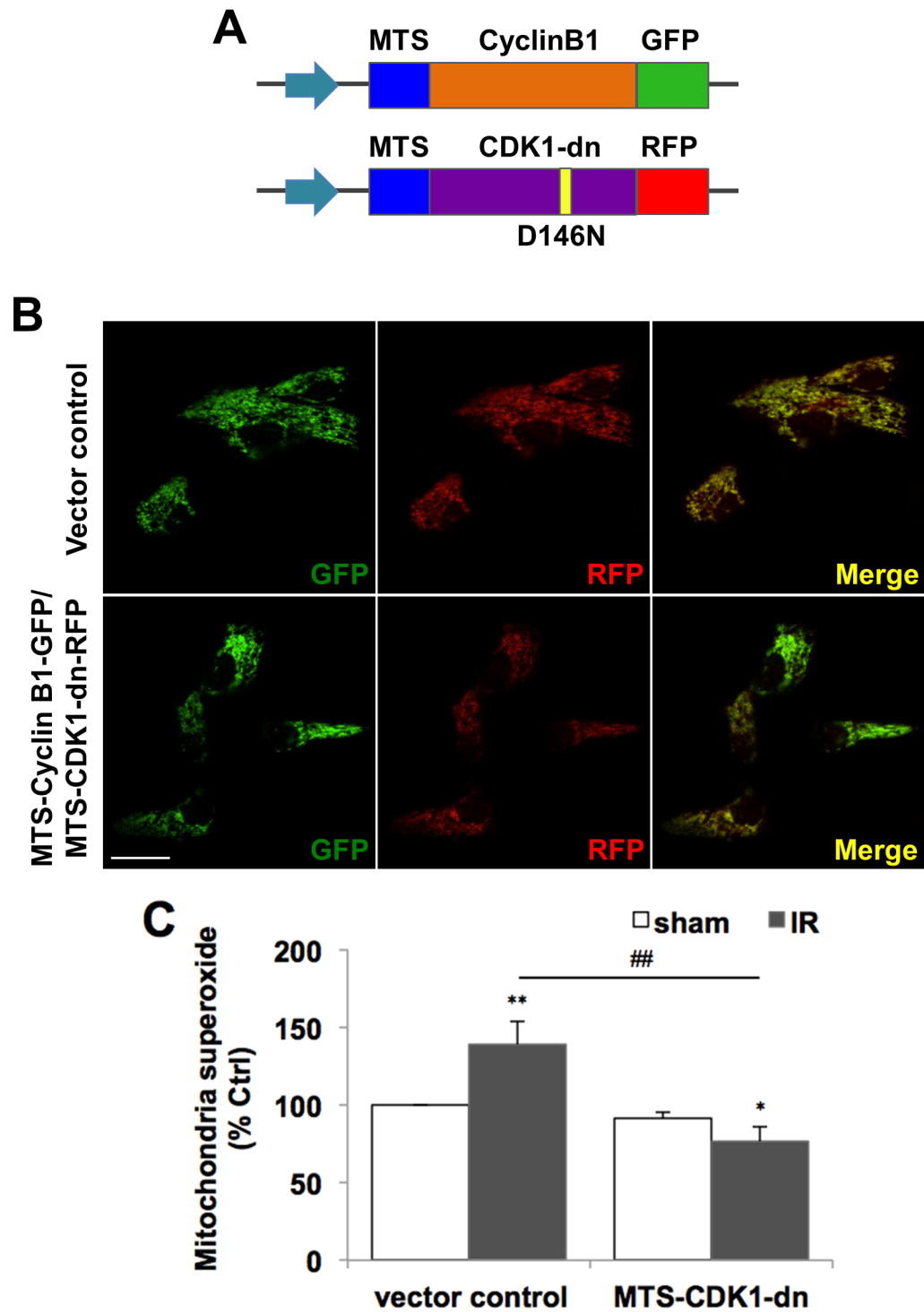# Figure S1

A

B

Figure S2

Figure S3

Figure S4

Supplemental Figure Legends

Figure S1. Cellular response of MCF10A cells to ionizing radiation, related to Figure 1. Cells were treated with 5 Gy radiation and mitochondrial superoxide levels (A) and MnSOD activity (B) were measured at the indicated time intervals post radiation. Data represent mean $\pm$ S.E.M.; *, $P < 0.05$; **, $P < 0.01$ irradiated cells vs. non-irradiated sham control cells; #, $P < 0.05$; $n = 3$.

Figure S2. Radiation induced DNA damage repair, cell cycle G2/M arrest and apoptosis, related to Figure 2. A, Radiation-induced foci formation. Images show γH2A.X foci formation at the indicated time intervals following 5 Gy irradiation. Scale bar, 20 μm. B, NHEJ DNA repair pathway in early phase of cellular radiation response tested by 53BP1 foci formation assay. Scale bar, 20 μm. C, Cell cycle distribution of irradiated cells were tested by Flow cytometry and data show percentage of cells analyzed with FlowJo software. D. Radiation-induced apoptosis tested by flow cytometry. Data show percentage of Annexin-positive cells analyzed with FlowJo software. Data represent mean $\pm$ S.E.M.; *, $P < 0.05$; **, $P < 0.01$; $n = 3$. E, Radiation-induced apoptosis indicated by western blotting of caspase-3.

Figure S3. Radiation induced mitochondrial relocation of Cyclin B1 and CDK1, related to Figure 3. A, Coordination of enhanced mitochondrial ATP generation, enhanced CDK1 mitochondrial relocation and DNA repair in irradiated MCF10A cells. Empty bar, fold changes in mitochondrial ATP generation; gray bar, fold changes in mitochondrial CDK1 protein level; black bar, percentage of cells with more than 3 foci in nucleus. B, Radiation induced Cyclin B1 expression and CDK1 activity. C, Purity of mitochondrial, nuclear and cytosolic fractions isolated from irradiated MCF10A cells tested by western blotting. Alpha-tubulin serves as cytosolic protein marker, Histone H3 serves as nuclear protein marker and COX IV serves as

mitochondrial protein marker. D, Radiation-enhanced mitochondrial relocation of CDK1 tested by transmission electron microscopy. Gold-labeled antibody was used to stain and visualize mitochondria-localized CDK1 (black dot). Scale bar, 0.2 μm. E, Mitochondrial localization of Cyclin B1 and CDK1 tested by immunostaining of Cyclin B1 (green, top panel) and CDK1 (green, middle panel). MitoTracker Red (red) and COX IV (green, bottom panel) serve as mitochondrial markers. Scale bar, 20 μm. F, Dose effect of ionizing radiation on mitochondria relocation of Cyclin B1 and CDK1. Mitochondrial fractions were isolated from cells receiving 2 Gy, 5 Gy or 8 Gy radiation and subjected to western blotting using antibodies against Cyclin B1 and CDK1. COXIV, mitochondria loading control. G, Expression of GFP-tagged mitochondrial respiration chain CI NDUFV3 in MCF10A cells. Cells were transfected with wild type or CDK1 phosphorylation deficient mutant NDUFV3. Images show the expression of GFP-tagged NDUFV3 24 h after transfection. Magnification, 10 × (left) and 16 × (Right).

Figure S4. Mitochondria targeting expression of Cyclin B1 and CDK1 in MCF10A cells, related to Figure 4. A, Schematic show of DNA constructs for mitochondria targeting expression of wild type Cyclin B1 and kinase activity deficient CDK1 (CDK1-dn). MTS, mitochondria targeting sequence. B, Confocal images showing mitochondria targeting expression of Cyclin B1 (green) and CDK1-dn (red) in cells 24 h after transfection. Scale bar, 20 μm. C, Cells were transfected with mitochondria-targeted Cyclin B1 and kinase deficient mutant CDK1 (MTS-CDK1-dn; dominant negative) for 24 h, and mitochondria superoxide levels were measured 24 h after 5 Gy radiation. Data represent mean ± S.E.M.; *, $P < 0.05$; **, $P < 0.01$ irradiated vs. non-irradiated sham control cells; ##, $P < 0.01$ MTS-CDK1-dn vs. empty vector control cells; n = 3.

Supplemental Experimental Procedures

Cell Culture and Treatment

MCF-10A cells, spontaneously immortalized human breast epithelial cells, were maintained in DMEM/F12 medium (HyClone, Logan, UT) supplemented with 5% horse serum (HyClone), 1% penicillin/streptomycin (containing 100 units/ml of penicillin and 100 μg/ml of streptomycin), 20 ng/ml EGF, 100 ng/ml Cholera toxin, 0.5 μg/ml hydrocortisone and 10 μg/ml insulin (Soule et al., 1990). P+JB6 mouse skin epidermal cells were maintained in MEM medium (HyClone) supplemented with 5% FBS (Gibco) and 1% penicillin/streptomycin. Human skin keratinocytes (HK18) were maintained in DMEM medium (HyClone) supplemented with 10% FBS and 1% penicillin/streptomycin. All cells were cultured in an incubator at 37°C, 5% CO_2 and 95% humidity. Exponentially grown cells were irradiated with a cabinet x-ray System Faxitron Series at a dose rate of 1.382 Gy/min (total 5 Gy) (Hewlett Packard).

Antibodies and Reagents

For western blotting, rabbit polyclonal anti-Cyclin B1 (1:500), anti-CDK1 (1:500) and anti-Ku80 (1:500) antibodies, mouse monoclonal anti-caspase 3, and goat anti-K70 (1:500) and anti-Rad51 (1:250) antibodies were obtained from Santa Cruz. Rabbit anti-γH2A.X (1:250), anti-pT161-cdc2 (1:500), anti-COX IV (1:1000) antibodies were purchased from Cell Signaling Technology. Rabbit anti-pT2609-DNA-PKcs (1:250) antibody was a gift from Prof. Zhengkun Luo. Mouse monoclonal anti-α-tubulin (1:5000), anti-β-actin (1:12000) antibodies were from Sigma. HRP-conjugated goat anti-mouse and anti-rabbit secondary antibodies (1:12000) were from Invitrogen. For foci formation assay, mouse anti-γH2A.X (1:200) was from Upstate. Rabbit anti-53BP1 (1:200) was from Cell Signaling Technology. Goat anti-Rad51 antibody (1:250) was obtained from Santa Cruz. Alexa-Fluor 488 conjugated goat anti-mouse (1:200), Cy5 conjugated donkey

anti-goat and goat anti-mouse secondary antibodies (1:200) were from Invitrogen. Rhodamine conjugated goat anti-rabbit (1:200) was from Jackson Immunoresearch Lab. ATP determination kit, MitoSOX and JC-1 were from Invitrogen. Comet assay kit was from Trevigen.

Measurement of Mitochondrial ATP Production

Mitochondrial ATP production was measured following published method (Vives-Bauza et al., 2007) with modifications. In brief, cells grown in 96-well plates were washed with ice-cold 1 x PBS (pH 7.4) and permeablized in ice-cold digitonin (25 µg/ml) for 1 min at the indicated time intervals after radiation. Cells were then washed with ice-cold 1 x PBS and incubated with 30 µl of buffer containing P1,P5-di(adenosine pentaphosphate) (0.15 mM), ADP (0.1 mM), malate (1 mM) and pyruvate (1 mM) with/without oligomycin (1 µg/ml) at room temperature for 5 min. An equal volume of 5% trichloroacetic acid was added to cells and incubated on ice for 20 min with gentle shaking. ATP extracts were then neutralized by adding 250 mM Tris-Acetate (pH 7.75) buffer and measured using ATP determination kit following the manufacturer's instructions.

MnSOD Activity

MnSOD activity assay was performed as previously described (Spitz and Oberley, 1989). Briefly, cells were lysed in DETAPAC buffer (1.34 mmol/L diethylenetriaminepentaacetic acid in 50 mM potassium phosphate buffer), sonicated with six times 5-sec bursts on ice, and centrifuged at 800g for 5 min at 4°C. The supernatant was transferred to a new tube and used immediately or stored at -80°C for future use. 5-50 µg of each sample was used for measurement of MnSOD activity at room temperature in assay solution (DETAPAC buffer containing 0.13 mg/ml BSA, 1.25 U/ml of catalase, 50 µM xanthine, 50 µM bathocuproinedisulfonic acid, 74.6 µM nitroblue tetrazolium (NBT)) in the presence of 5 mM sodium cyanide (NaCN) to inhibit CuZnSOD

activity in a 96-well plate. The assay reaction was initiated by adding xanthine oxidase and incubated at 37°C for 30 min. The OD absorbance at 560 nm was monitored with the Spectra Max M2e plate reader (Molecular Devices Co.) every 30 sec for 5 min. MnSOD activity was calculated as the amount of protein inhibiting NBT reduction by 50% and presented as percent changes compared to control.

Measurement of Mitochondrial Superoxide

Cells (1.5×10^4) seeded in a 96-well plate were washed with pre-warmed $1 \times$ PBS, pH 7.4 twice and incubated in 100 µl of MitoSOX Red working solution (final concentration of 5 µM diluted from a 5 mM stock solution in DMSO with PBS) for 10 min at 37°C. Cells were then washed with PBS twice and the fluorescence intensity was monitored directly in PBS using microplate reader (Spectra Max M2e) at 510 nm/580 nm wavelength (excitation/emission). The mitochondrial superoxide was shown as percent of fluorescence intensity generated in control cells.

Flow Cytometry

To determine cell cycle distribution, cells were collected by trypsinization, fixed in ice-cold 70% ethanol, and stained in PBS containing 50 µg/ml propidium iodide (Sigma), 0.1 mg/ml BSA, 0.1%, v/v Triton X-100 and 0.2 mg/ml DNase-free RNase for 10 min in the dark at room temperature. For apoptosis assay, cells were trypsinized, washed and resuspended in Annexin V binding buffer at concentration of $0.5\sim1 \times 10^6$ cells. An aliquot of 100 µl cells were then stained in flow tubes in binding buffer containing 5 µl Annexin V (BD Pharmingen) and 50 µg/ml propidium iodide for 10 min in the dark at room temperature. Cell cycle distribution and apoptosis were analyzed by flow cytometry using a FCA Calibur instrument (Becton Dickinson, Mountain View, CA) and the data were analyzed using FlowJo vX.0.7 analysis program.

Immunoelectron Microscopy

Immunoelectron microscopy analysis was performed as described previously (Tait et al., 2000). Briefly, cells were fixed in ice-cold 4% paraformaldehyde, 0.1% glutaraldehyde in 0.1 M phosphate buffer (pH 7.4) for 30 min. Cells were then incubated in 0.1% tannic acid, 1% uranyl acetate to increase the preservation and contrast and dehydrated in an ethanol dehydration series (50%, 70%, 80%, 90% and 100%; 5 min each). Cells were infiltrated in LR White resin (Agar Scientific Ltd.), embedded in gelatin capsules and polymerized using clinical microwave. The embedded samples were then cut into 60 nm ultrathin sections and the sections were mounted on the nickel Grids. Grids were blocked in 1% BSA for 30 min and incubated with anti-CDK1 antibody for 2 h followed by incubation with 10 nm gold-conjugated secondary antibody for 1 h at room temperature. Grids were then stained in uranyl acetate and lead citrate and the images were acquired using transmission microscope (Philips CM120, Biotwin Lens, model 794/20, digital camera of 2K × 2K).

Gene Silencing by siRNA

SiRNAs targeting Cyclin B1 (sense sequence: 5'-AATTTCTGGAGGGTACATTTCCCTGTCTC-3', antisense sequence: 5'-AAGAAATGTACCCTCCAGAAACCTGTCTC-3') and CDK1 (sense sequence: 5'-AAGGGGTTCCTAGTACTGCAACCTGTCTC -3'; antisense sequence: 5'-AATTGCAGTACTAGGAACCCCCCTGTCTC -3') mRNA were synthesized using the Silencer siRNA construction kit (Ambion). Exponentially grown cells were transfected with 30 nM siRNA using LipofectamineTM RNAi MAX following the manufacturer's instructions for 24 h. Scramble siRNAs (sense sequence: 5'-AAATATGTGCGTACCTAGCTTCCTGTCTC-3'; antisense sequence: 5'-AAGCTAGGTACGCACATATTTCCTGTCTC-3') were used as control.

Supplemental References

Soule, H.D., Maloney, T.M., Wolman, S.R., Peterson, W.D., Jr., Brenz, R., McGrath, C.M., Russo, J., Pauley, R.J., Jones, R.F., and Brooks, S.C. (1990). Isolation and characterization of a spontaneously immortalized human breast epithelial cell line, MCF-10. Cancer Res. *50*, 6075-6086.

Spitz, D.R., and Oberley, L.W. (1989). An assay for superoxide dismutase activity in mammalian tissue homogenates. Anal. Biochem. *179*, 8-18.

Tait, S., Gunn-Moore, F., Collinson, J.M., Huang, J., Lubetzki, C., Pedraza, L., Sherman, D.L., Colman, D.R., and Brophy, P.J. (2000). An oligodendrocyte cell adhesion molecule at the site of assembly of the paranodal axo-glial junction. J. Cell Biol. *150*, 657-666.

Vives-Bauza, C., Yang, L., and Manfredi, G. (2007). Assay of mitochondrial ATP synthesis in animal cells and tissues. Methods Cell Biol. *80*, 155-171.